JCI The Journal of Clinical Investigation

Carbohydrate-binding protein CLEC14A regulates VEGFR-2– and VEGFR-3–dependent signals during angiogenesis and lymphangiogenesis

Sungwoon Lee, … , Young-Myeong Kim, Young-Guen Kwon

Research Article Angiogenesis Vascular biology

Controlled angiogenesis and lymphangiogenesis are essential for tissue development, function, and repair. However, aberrant neovascularization is an essential pathogenic mechanism in many human diseases, including diseases involving tumor growth and survival. Here, we have demonstrated that mice deficient in C-type lectin family 14 member A (CLEC14A) display enhanced angiogenic sprouting and hemorrhage as well as enlarged jugular lymph sacs and lymphatic vessels. CLEC14A formed a complex with VEGFR-3 in endothelial cells (ECs), and CLEC14A KO resulted in a marked reduction in VEGFR-3 that was concomitant with increases in VEGFR-2 expression and downstream signaling. Implanted tumor growth was profoundly reduced in CLEC14A-KO mice compared with that seen in WT littermates, but tumor-bearing CLEC14A-KO mice died sooner. Tumors in CLEC14A-KO mice had increased numbers of nonfunctional blood vessels and severe hemorrhaging. Blockade of VEGFR-2 signaling suppressed these vascular abnormalities and enhanced the survival of tumor-bearing CLEC14A-KO mice. We conclude that CLEC14A acts in vascular homeostasis by fine-tuning VEGFR-2 and VEGFR-3 signaling in ECs, suggesting its relevance in the pathogenesis of angiogenesis-related human disorders.

Find the latest version:

https://jci.me/85145/pdf

Carbohydrate-binding protein CLEC14A regulates VEGFR-2– and VEGFR-3–dependent signals during angiogenesis and lymphangiogenesis

Sungwoon Lee,[1] Seung-Sik Rho,[1] Hyojin Park,[1] Jeong Ae Park,[1] Jihye Kim,[1] In-Kyu Lee,[2] Gou Young Koh,[3] Naoki Mochizuki,[4] Young-Myeong Kim,[5] and Young-Guen Kwon[1]

[1]Department of Biochemistry, College of Life Sciences and Biotechnology, Yonsei University, Seoul, South Korea. [2]Department of Internal Medicine, Kyungpook National University School of Medicine and Leading-edge Research Center for Drug Discovery and Development for Diabetes and Metabolic Disease, Kyungpook National University Medical Center, Daegu, South Korea. [3]Graduate School of Medical Science and Engineering, Korea Advanced Institute of Science and Technology, Daejeon, South Korea. [4]Department of Cell Biology, National Cerebral and Cardiovascular Center Research Institute, Osaka, Japan. [5]Vascular System Research Center, Kangwon National University, Chunchon, South Korea.

Controlled angiogenesis and lymphangiogenesis are essential for tissue development, function, and repair. However, aberrant neovascularization is an essential pathogenic mechanism in many human diseases, including diseases involving tumor growth and survival. Here, we have demonstrated that mice deficient in C-type lectin family 14 member A (CLEC14A) display enhanced angiogenic sprouting and hemorrhage as well as enlarged jugular lymph sacs and lymphatic vessels. CLEC14A formed a complex with VEGFR-3 in endothelial cells (ECs), and CLEC14A KO resulted in a marked reduction in VEGFR-3 that was concomitant with increases in VEGFR-2 expression and downstream signaling. Implanted tumor growth was profoundly reduced in CLEC14A-KO mice compared with that seen in WT littermates, but tumor-bearing CLEC14A-KO mice died sooner. Tumors in CLEC14A-KO mice had increased numbers of nonfunctional blood vessels and severe hemorrhaging. Blockade of VEGFR-2 signaling suppressed these vascular abnormalities and enhanced the survival of tumor-bearing CLEC14A-KO mice. We conclude that CLEC14A acts in vascular homeostasis by fine-tuning VEGFR-2 and VEGFR-3 signaling in ECs, suggesting its relevance in the pathogenesis of angiogenesis-related human disorders.

Introduction

Angiogenesis and lymphangiogenesis are essential for proper tissue development, but neovascularization can facilitate the progression of pathological conditions, such as tumor growth and survival. VEGFs and two of their receptors (VEGFR-2 and VEGFR-3) are critical factors mediating developmental angiogenesis and lymphangiogenesis, along with pathological angiogenesis. Endothelial deletion of VEGFR-2 or VEGFR-3 disrupts VEGFR-2/-2, VEGFR-2/-3, and VEGFR-3/-3 signaling complexes, leading to cardiovascular failure, abnormal vessel formation in the postnatal retina, or aberrant tumor vessel formation. Activation of VEGFR-2 induces VEGFR-3 expression, whereas silencing of *Vegfr3* promotes VEGFR-2 phosphorylation in blood vessels (1–4). This mutual regulation acts to control the activation of Notch/DLL4 signaling, a key effector pathway for vascular sprouting and patterning (4, 5).

VEGF/VEGFR signaling also contributes to tumor development by regulated angiogenesis. However, the tumor microcirculation exhibits abnormal characteristics, such as excessive and tortuous vessels, leakiness, and lack of pericyte coverage; these observations have stimulated the search for therapeutic agents that inhibit tumor angiogenesis (6, 7). Although targeting VEGF/VEGFRs has been successful in inhibiting certain tumors, it has inconsistent and incomplete effects on the vasculature of other tumors and does not improve outcomes. Therefore, understanding the molecular mechanisms underlying angiogenic VEGF/VEGFR signaling could facilitate the development of targeted molecular therapies to enhance tumor destruction, while allowing for normal angiogenesis of nontumor tissues.

C-type lectin family 14 member A (CLEC14A) is a type I transmembrane protein belonging to the C-type lectin superfamily that contains an EGF-like domain, along with the C-type lectin domain (8). The C-type lectin domain is a carbohydrate-binding protein domain that mediates many functions including cell-to-cell adhesion, inflammatory responses, and apoptosis (9–12). Many C-type lectin superfamily proteins are receptors found in immune cells such as DCs, macrophages, neutrophils, monocytes, and B cells. Binding of these receptors to pathogens activates distinct signaling pathways that shape the immune response (13). Previously, we found that CLEC14A is upregulated during the morphogenesis of endothelial progenitor cells into endothelial cells (ECs) (14). Recently, SILAC-based (stable isotope labeling with amino acids in cell culture–based) proteomics revealed that CLEC14A expression is enhanced in ECs during tubule morphogenesis and regulates cell–extracellular matrix adhesion to multimerin 2 (MMRN2), a suppressor of VEGF/VEGFR signaling during angiogenesis (15). Moreover, CLEC14A expression was significantly higher in the blood vessels of the tumor than in those of adjacent normal tissue (16), along with robust detection in tumor ECs and
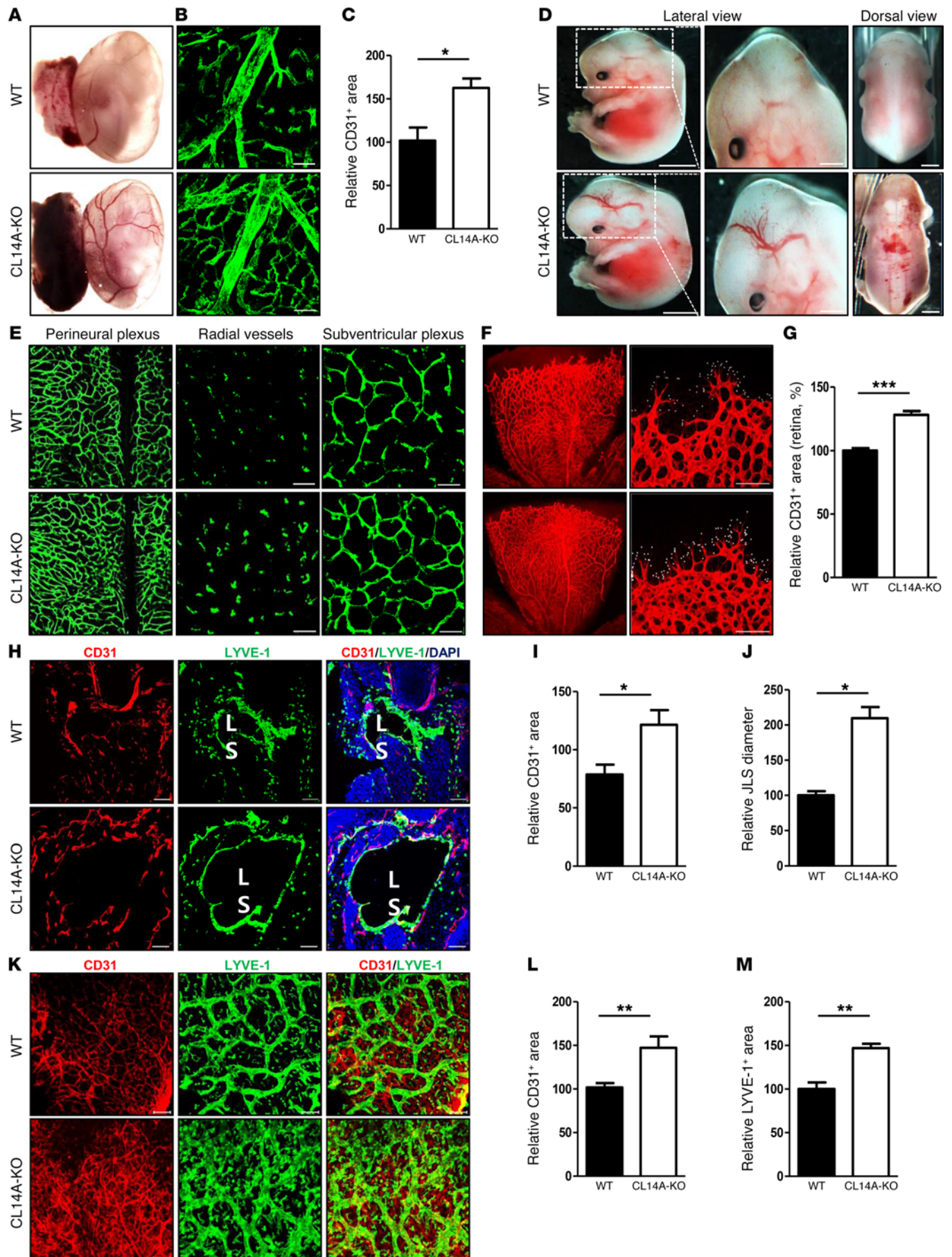
Figure 1. CLEC14A is specifically expressed in blood and lymphatic ECs, and loss of CLEC14A increases developmental angiogenesis and lymphangiogenesis. (A) Images of unfixed E13.5 yolk sacs from WT and CLEC14A-KO mice. *n* = 10 per group. Scale bar: 200 μm. **(B)** Whole-mount CD31 immunostaining of yolk sacs from WT and CLEC14A-KO mice. *n* = 10 per group. Scale bars: 100 μm. **(C)** Quantification of CD31 immunostaining of E13.5 yolk sacs (percentage of control). **(D)** Lateral and dorsal views of unfixed E13.5 WT and CLEC14A-KO embryos. *n* = 10 per group. Scale bars: 100 μm. **(E)** Immunostaining of flat-mount preparations of E13.5 hind brains from WT and CLEC14A-KO mice. Each layer of vessels in the hind brain is displayed according to the radial position. *n* = 6 per group. Scale bars: 100 μm. **(F)** Whole-mount preparations of P5 retinae from WT and CLEC14A-KO pups immunostained for CD31 (white dots represent individual filopodia). *n* = 10 per group. Scale bars: 100 μm. **(G)** Quantification of relative vascular density (percentage of control). **(H)** Transverse sections of E15.5 WT and CLEC14A-KO embryos immunostained for CD31 and LYVE-1. *n* = 6 per group. Scale bars: 100 μm. JLS: Jugular Lymph Sac. **(I and J)** Quantification of relative vascular density and diameter of JLS (percentage of control) **(K)** Flat-mount preparations of E15.5 WT and CLEC14A-KO forelimbs immunostained for CD31 and LYVE-1. *n* = 6 per group. Scale bars: 100 μm. **(L and M)** Quantification of relative lymphatic vessel density and diameter of the lymphatic vessels (percentage of control). All experiments were repeated on at least 6 different sets of WT and KO littermates. *P < 0.05, **P < 0.005, and ***P < 0.0001, by paired, 2-tailed Student's *t* test. Error bars represent the mean ± SD.

under hypoxic conditions as well as in circulating ECs of cancer patients (8, 16–18). Furthermore, CLEC14A regulates sprouting angiogenesis by shedding its ectodomain, which is catalyzed by rhomboid-like 2 protein (19).

These results strongly suggest that CLEC14A participates in tumor angiogenesis, but detailed functional analyses are lacking. Here, we evaluated CLEC14A functions in developmental angiogenesis and lymphangiogenesis as well as pathological angiogenesis using *Clec14a⁻/⁻* mice (referred to herein as CLEC14A-KO mice). Our data demonstrated that CLEC14A contributes to vascular sprouting and stability during angiogenesis and to the formation of normal lymph sac and lymphatic vasculature by modulating VEGFR-3 and VEGFR-2 expression levels and signaling.

Results

Generation of CLEC14A-KO mice and evaluation of vessel-specific CLEC14A expression. To investigate CLEC14A function in angiogenesis, we established KO mice by replacing the entire *Clec14a* gene with the β-galactosidase (β-gal) gene, while retaining upstream and downstream regulators through homologous recombination (Supplemental Figure 1A; supplemental material available online with this article; doi:10.1172/JCI85145DS1). We verified replacement of the WT CLEC14A-encoding genomic DNA segment by genotyping PCR (Supplemental Figure 1B and Supplemental Table 1). Global CLEC14A-KO mice were viable and fertile. Deletion of *Clec14a* was confirmed by immunostaining for CD31 and CLEC14A with 2 different antibodies, N-terminal and C-terminal antibodies (Supplemental Figure 1C). Real-time PCR (RT-PCR) analysis of 5′-UTR, CDS, and 3′-UTR regions showed deletion of the CDS region of *Clec14a* (Supplemental Figure 1D and Supplemental Table 2). Lung lysates of WT and CLEC14A-KO littermates showed complete deletion of *Clec14a* at the protein level (Supplemental Figure 1E). X-gal staining at E10.5 revealed intense vascular expression of the β-gal gene in the internal carotid artery,

dorsal aorta, and intersomitic vessels (Supplemental Figure 2A). CLEC14A-KO adult mice showed high β-gal activity in the vessels of the brain, retina, liver, lungs, lymph nodes, and ears (Supplemental Figure 2B). We confirmed the blood vessel specificity of CLEC14A expression in several organs of 5-week-old WT mice, including the retinae, brain, and lungs, by dual immunostaining for CLEC14A and the blood vessel endothelial marker CD31 (Supplemental Figure 2C). We also confirmed lymphatic vessel specificity of CLEC14A expression by immunostaining for lymphatic vessel endothelial hyaluronan receptor (LYVE-1) and CLEC14A in the forelimbs of E13.5 WT mice (Supplemental Figure 2D). These data suggest that CLEC14A is specifically expressed in the blood and lymphatic endothelial vessels.

CLEC14A KO results in increased angiogenesis and lymphangiogenesis during embryonic and postnatal development. To examine the function of CLEC14A expression during developmental angiogenesis, enucleated yolk sacs from E13.5 mice were examined by microscopic inspection and immunostaining for CD31. Compared with WT mice, yolk sacs from CLEC14A-KO mice exhibited elevated microvessel density on visual inspection (Figure 1A), as confirmed by CD31 immunostaining (Figure 1, B and C). Hemorrhages and dilated vessels were present in the hind brain and dorsal regions of E13.5 CLEC14A-KO mice but not in those of WT embryos (Figure 1D). Despite hemorrhages during embryonic development, CLEC14A-KO mice were viable, indicating compensatory mechanisms for CLEC14A loss. Histological analysis of flat-mount preparations of E13.5 brains from CLEC14A-KO mice revealed a higher density and enlargements of vessels in the perineural, radial, and subventricular plexus regions of the hind brain (Figure 1E). Sagittal sections of E13.5 brains from CLEC14A-KO mice also showed reduced pericyte coverage, as indicated by reduced immunostaining for the pericytic marker NG2, and increased vessel density, as indicated by CD31 staining (Supplemental Figure 3, A–C). Whole-mount preparations of P5 retinae from CLEC14A-KO mice demonstrated increased vessel density, numerous branch points and filopodia projections, and a greater proliferation of retinal vessels (Figure 1, F and G, and Supplemental Figure 3, D–H). Furthermore, pericyte coverage was reduced, as indicated by a lower NG2/CD31 staining ratio, and red blood cells were present at the vascular front, indicating vessel leakage (Supplemental Figure 3, I and J). Regarding the lymphatic vessel–specific expression of CLEC14A, we examined lymphatic vessels and jugular lymph sacs during embryogenesis. Whole-mount preparations of E11.5 embryo forelimbs of CLEC14A-KO revealed an increase in vessel density and lymphatic vessel density (Supplemental Figure 4A). Transverse sections of E13.5 and E15.5 CLEC14A-KO mice showed an enlarged jugular lymph sac diameter, as indicated by immunostaining for LYVE-1 (Supplemental Figure 4, B–D and Figure 1, H–J). Flat-mount preparations of E13.5 and E15.5 forelimbs from CLEC14A-KO mice showed increased vessel density and diameter (Supplemental Figure 4, E–G and Figure 1, K–M). These data suggest that CLEC14A is involved in EC sprouting and the integrity of angiogenic blood and lymphatic vessels.

CLEC14A deficiency increases VEGF-A–dependent EC sprouting and vessel density. To examine the effects of CLEC14A deficiency on EC sprouting and angiogenesis in the absence of confounding factors, we performed ex vivo aortic ring assays and Matrigel plug
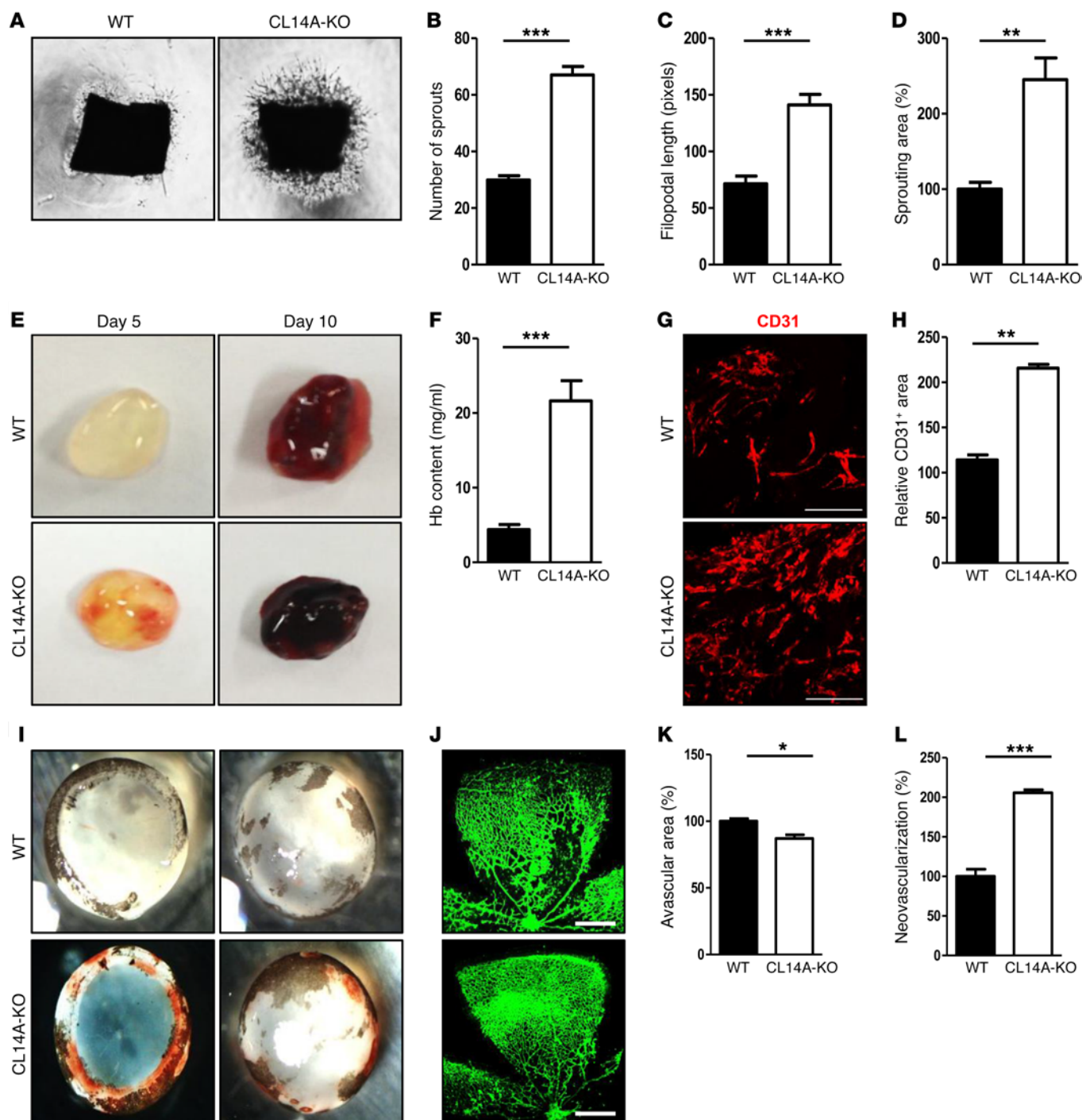
Figure 2. Deletion of *Clec14a* results in increased development of poorly functional (hemorrhage-prone) vessels. (**A**) Murine aortic ring assay for P7 WT and CLEC14A-KO mice (VEGF-A; 50 ng). *n* = 3 per group. Magnification ×10. (**B–D**) Quantification of the number of sprouts, filopodial length, and relative sprouting area (percentage of control). (**E**) Matrigel plugs implanted into 7-week-old WT and CLEC14A-KO mice for 5 or 10 days. *n* = 6 per group. (**F**) Quantification of Hb (mg/ml) extracted from Matrigel plugs from WT and CLEC14A-KO mice. *n* = 6 per group. (**G**) CD31 immunostaining of Matrigel plugs implanted into WT and CLEC14A-KO mice for 10 days. Scale bars: 100 μm. (**H**) Quantification of the relative CD31-positive area (percentage of control). (**I**) Hemorrhage in P17 WT and CLEC14A-KO mouse retinae after hyperoxia (OIR model). *n* = 3 per group. (**J**) Whole-mount isolectin B (green) staining of P17 retinae from WT and CLEC14A-KO mice. Scale bars: 500 μm. (**K** and **L**) Relative avascular and neovascularization areas in P17 retinae from WT and CLEC14A-KO mice (percentage of control). All experiments were repeated on at least 3 different sets of WT and KO littermates. *$P < 0.05$, **$P < 0.005$, and ***$P < 0.0001$, by paired, 2-tailed Student's *t* test. Error bars represent the mean ± SD.

assays. Aortic rings from P7 WT and CLEC14A-KO mice were isolated and embedded in Matrigel containing VEGF-A. The assay demonstrated a greater proliferation and extension of mouse EC sprouts from the aortic rings of CLEC14A-KO mice than from those of WT mice (Figure 2, A–D). Matrigel mixed with VEGF-A was then injected s.c. into 6-week-old WT and CLEC14A-KO mice and removed on day 5 or day 10. Angiogenesis occurred earlier and was more extensive in the Matrigel plugs from CLEC14A-KO mice (Figure 2E). Moreover, these plugs contained more hemoglobin (Hb), consistent with greater numbers of invading blood vessels (Figure 2F). Confocal images of cryosectioned Matrigel plugs confirmed an increased CD31-positive area in the plugs from CLEC14A-KO mice compared with those from WT mice (Figure 2, G and H). Taken together, our data suggest that loss of CLEC14A accelerates angiogenesis in response to VEGF-A.

Oxygen-induced retinopathy results in severe hemorrhage and hypervascularity in CLEC14A-KO mice. To investigate the effect of *Clec14a* deletion during pathological angiogenesis, we examined the oxygen-induced retinopathy (OIR) model. Retinopathy due to prematurity-associated vascular dysfunction is treated clinically by inhibiting VEGF-A/VEGFR-2 signaling (20). Following hyperoxic treatment for 5 days, we detected severe hemorrhage in retinae from CLEC14A-KO mice but not in those from WT mice (Figure 2I). Quantification of retinal blood vessels immunostained with isolectin B4 revealed a reduced avascular area in the retinae of CLEC14A-KO mice compared with retinae of WT mice, consistent with elevated neovascularization (Figure 2, J–L). Thus, deletion of *Clec14a* led to increased retinal vascularization under hyperoxic conditions, conferring greater vulnerability to pathological sequelae such as retinal hemorrhage.

Loss of CLEC14A attenuates VEGFR-3 expression and enhances VEGFR-2 expression. The angiogenic phenotypes of CLEC14A-KO mice were similar to those of endothelium-specific VEGFR-3–KO mice. In a previous study, EC-specific deletion of *VEGFR-3* induced hypervascularity in angiogenic vessels, whereas VEGFR-3 knockdown using siRNA, followed by VEGF treatment, increased the level of VEGFR-2 phosphorylation in HUVECs (5). Hence, we hypothesized that CLEC14A regulates angiogenesis by influencing VEGFR-3 expression or activity, thereby altering VEGFR-2 activity as well. To assess the relationship among CLEC14A, VEGFR-3, and VEGFR-2, we silenced CLEC14A in HUVECs. This treatment resulted in decreased VEGFR-3 mRNA and protein levels and increased VEGFR-2 mRNA and protein levels (Figure 3, A–D), suggesting that enhanced angiogenesis in CLEC14A-KO mice results from reduced VEGFR-3 signaling and hyperactivation of VEGFR-2 signaling. Given that silencing of VEGFR-3 decreases *Notch/Dll4* and Notch target gene expression (5), we evaluated *Notch/DLL4* and target gene expression in HUVECs following CLEC14A knockdown. CLEC14A knockdown suppressed *Notch/DLL4* and Notch target gene expression, demonstrating reduced VEGFR-3 signaling (Supplemental Figure 5A and Supplemental Table 3).

Next, we examined the expression levels of VEGFR-3 and VEGFR-2 in CLEC14A-KO mouse embryos and retinae. Flatmount preparations of P5 retinae showed elevated vessel density, weaker VEGFR-3 expression, and more intense VEGFR-2 expression at the vascular front in CLEC14A-KO retinae (Figure 3, E–H), along with lower VEGFR-3 and elevated VEGFR-2 immu-

noexpression in the intercarotid artery and intersomitic vessels of whole-mount preparations of E10.5 CLEC14A-KO embryos (Supplemental Figure 5, B and C). To confirm that these inverse expression patterns were specific to ECs, we compared VEGFR subtype protein expression levels in aortal and retinal lysates as well as mRNA expression levels in isolated murine lung ECs (MLECs) and hyaloid vessels from WT and CLEC14A-KO mice. Similar to the immunostaining results, VEGFR-3 expression was reduced and VEGFR-2 expression was elevated in CLEC14A-KO mouse retinal lysates relative to retinal lysates from WT mice (Figure 3I) and aortal lysates (Figure 3J). Consistent with previous results, *VEGFR-3* mRNA expression levels were reduced and *VEGFR-2* mRNA expression levels were increased, and *Notch/Dll4* and Notch target gene expression levels were also reduced in both MLECs and hyaloid vessels (Supplemental Figure 6, A–H).

To examine whether changes in VEGFR-3 also influence CLEC14A expression, VEGFR-3 expression was knocked down in HUVECs by siRNA. VEGFR-3 silencing attenuated CLEC14A expression levels and greatly potentiated VEGFR-2 expression (Figure 3K and Supplemental Figure 6, I–K). Thus, the expression levels of VEGFR-3 and CLEC14A changed in parallel, suggesting mutual upregulation, whereas loss of either one enhanced VEGFR-2 expression.

CLEC14A interacts with VEGFR-3 in ECs. We speculated that CLEC14A regulates VEGFR-3 and VEGFR-2 by interaction with one or both receptors at the protein level. IP indicated such an interaction between endogenous CLEC14A and VEGFR-3 but not with VEGFR-2, neuropilin 2, or ephrin B2, all of which are known to interact with VEGFR-3 (Figure 3L). To verify this interaction between CLEC14A and VEGFR-3, HUVECs were transfected with GFP-tagged CLEC14A. GFP-tagged CLEC14A formed a complex with VEGFR-3 but not VEGFR-2 (Figure 3M). Subsequent deletion mutant studies identified the cytosolic domain of CLEC14A as the binding region for VEGFR-3 (Figure 3N). The interaction of CLEC14A with VEGFR-3 was further substantiated by dual immunostaining of P5 WT retinal ECs, which showed overlapping expression in filopodia projections at the vascular front and in the vascular plexus regions (Supplemental Figure 6L). In light of previous results showing increased phosphorylation of VEGFR-2 upon silencing of VEGFR-3 in HUVECs (5) and impaired VEGFR-2 signaling by MMRN2, which binds to VEGF-A to negatively regulate VEGF/VEGFR-2 signaling (15), we examined the phosphorylation status of VEGFR-2 and expression levels of MMRN2 upon silencing of CLEC14A in the presence and absence of VEGF-A in HUVECs. We found that MMRN2 expression was decreased by CLEC14A silencing and VEGF-A treatment in a time-dependent manner (Supplemental Figure 7A). Phosphorylation of VEGFR-2 was enhanced by silencing of CLEC14A in the presence or absence of VEGF-A (Supplemental Figure 7B). These results suggest that CLEC14A interacts with VEGFR-3, controlling VEGFR-2 signaling together with VEGF-A and MMRN2.

CLEC14A regulates VEGF-C/VEGFR-3 and VEGF-A/VEGFR-2 signaling in both blood endothelial cells and LECs. In line with our previous results demonstrating a reduction of VEGFR-3 and induction of VEGFR-2 upon CLEC14A silencing and previous studies reporting regulation of ERK via the molecular control of VEGFR-3 and VEGFR-2, we further evaluated VEGFR-3 and VEGFR-2 sig-
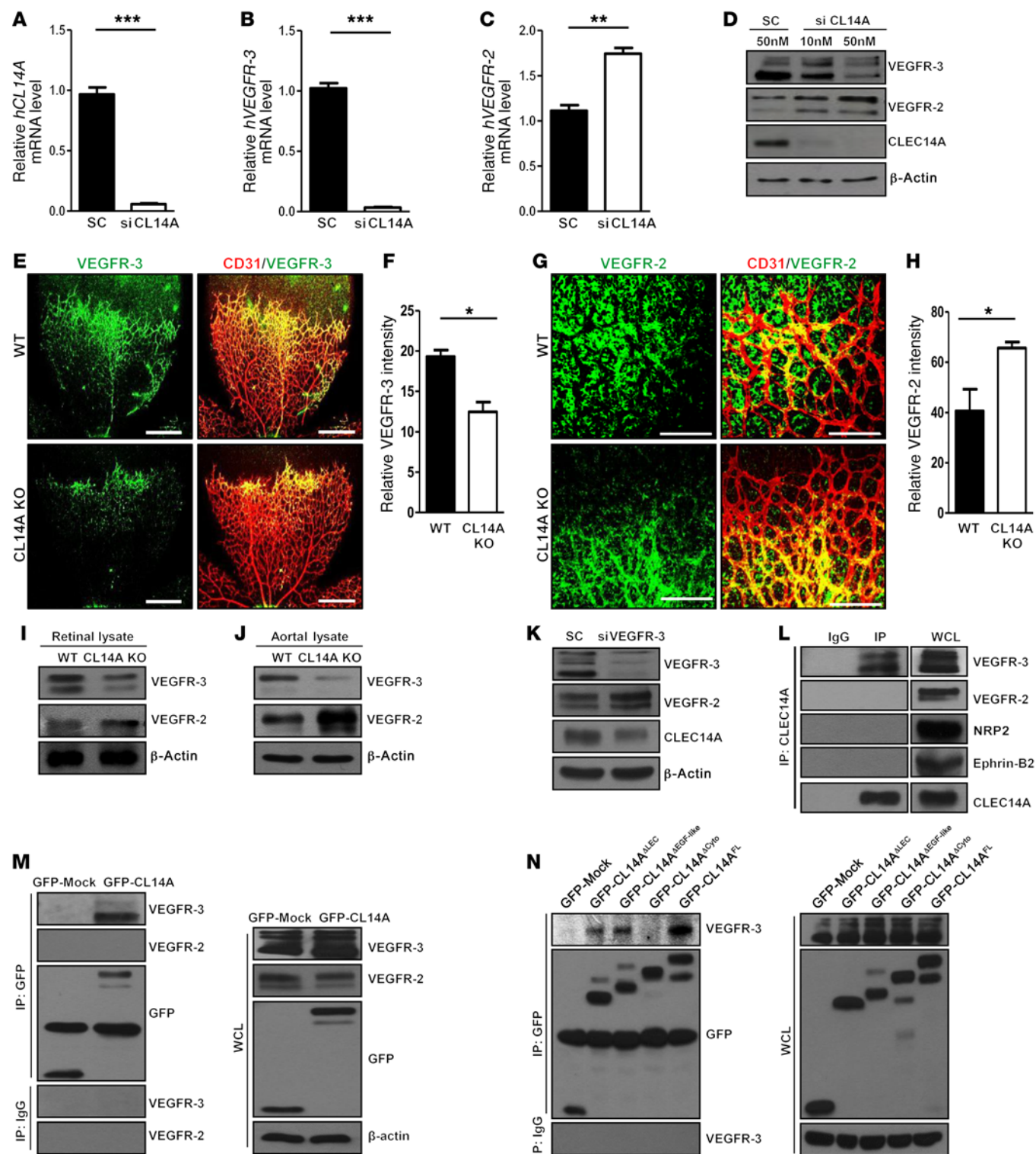
Figure 3. CLEC14A deficiency attenuates VEGFR-3 expression, promotes VEGFR-2 expression, and forms a CLEC14A–VEGFR-3 complex via the CLEC14A cytosolic domain in ECs. (**A**–**C**) Relative *GAPDH*-normalized mRNA levels of human *CLEC14A* (*hCLEC14A*), *hVEGFR-3*, and *hVEGFR-2* after CLEC14A silencing in HUVECs. (**D**) Reduced VEGFR-3 and increased VEGFR-2 protein expression in HUVECs after silencing of CLEC14A with 50 nM CLEC14A siRNA. (**E** and **F**) Confocal images and quantification of relative VEGFR-3 staining intensity in P5 retinae from WT and CLEC14A-KO mice, demonstrating reduced VEGFR-3 in CLEC14A-KO retinae (percentage of control). Scale bars: 500 μm. (**G** and **H**) Confocal images and quantification of relative VEGFR-2 intensity of P5 retinae from WT and CLEC14A-KO mice showing increased VEGFR-2 expression (percentage of control). *n* = 6 per group. Scale bars: 100 μm. (**I** and **J**) Decreased VEGFR-3 and increased VEGFR-2 protein expression in retinal and aortal lysates isolated from P5 WT and CLEC14A-KO pups. (**K**) VEGFR-3, CLEC14A, and VEGFR-2 protein expression in HUVECs after silencing of VEGFR-3 with 50 nM siRNA. VEGFR-3 silencing reduced CLEC14A expression and promoted VEGFR-2 expression. (**L**) Co-IP of endogenous CLEC14A with VEGFR-3 but not with VEGFR-2 in HUVECs. (**M**) IP assay showing that overexpressed GFP-tagged CLEC14A (GFP-CL14A) bound to VEGFR-3 but not to VEGFR-2 in HUVECs. Western blot shows transfection of GFP-Mock and GFP-CLEC14A in HUVECs. (**N**) *Clec14a* deletion series shows that VEGFR-3 interacted with the cytosolic domain of CLEC14A. IP analysis shows deletion mutants of GFP-tagged CLEC14A (GFP-Mock, GFP-CL14A-ΔLEC, GFP-CL14A-ΔEGF-like, GPF-CL14A-ΔCyto, and GFP-CL14A-FL) interacting with VEGFR-3. The deletion mutants were transfected into HUVECs and immunoprecipitated with anti-GFP antibody or IgG. Western blot analysis of cell lysates after transfection of each deletion mutant into HUVECs. All experiments were repeated at least 4 times with similar results. *P < 0.05, **P < 0.005, and ***P < 0.0001, by paired, 2-tailed Student's *t* test. SC, scrambled siRNA; FL, full-length; WB, Western blot; WCL, whole-cell lysate. Error bars represent the mean ± SD.

naling upon knockdown or overexpression of CLEC14A at optimal time points for VEGF-C (15 minutes) or VEGF-A (5 minutes) in both human dermal blood endothelial cells (HDBECs) and human dermal LECs (HDLECs). Phosphorylation of VEGFR-3 was reduced and phosphorylation of VEGFR-2 and VEGFR-2–mediated ERK was increased upon CLEC14A silencing when stimulated with VEGF-A for 5 minutes in both HDBECs and HDLECs (Figure 4A and Supplemental Figure 7C). VEGFR-3–mediated ERK phosphorylation was decreased upon CLEC14A silencing when stimulated with VEGF-C for 15 minutes in both HDBECs and HDLECs (Figure 4B and Supplemental Figure 7D). Overexpression of CLEC14A resulted in inverse patterns of VEGFR-3, VEGFR-2, and ERK signaling when stimulated with VEGF-C or VEGF-A in both HDBECs and HDLECs (Figure 4, C and D, and Supplemental Figure 7, E and F). Furthermore, phosphorylation of ERK was increased in aortal lysates from P6 CLEC14A-KO mice (Supplemental Figure 7G), suggesting a molecular mechanism of increased blood and lymphatic vessels and vessel enlargement, combined with increased phosphorylation of eNOS, and demonstrating enhanced VEGFR-2 signaling that led to increased permeability and proliferation in vivo (Supplemental Figure 7H). Consistent with the inverse pattern of VEGFR-3 and VEGFR-2 activation and expression levels, *VEGFR-3*, *Notch*, and Notch target gene mRNA expression levels were reduced and *VEGFR-2* mRNA expression levels were elevated by CLEC14A silencing in the presence of VEGF-A or VEGF-C in both HDBECs and HDLECs (Supplemental Figures 8 and 9). Furthermore, endocytosed VEGFR-3 was decreased in CLEC14A-deficient BECs and LECs upon VEGF-A and VEGF-C stimulation, while endocytosed VEGFR-2 was increased, suggesting that

Clec14a deletion does not determine the cell-surface expression of VEGFR-3 (Supplemental Figures 10–13). Thus, it can be concluded that the interaction between CLEC14A and VEGFR-3 modulates VEGFR-3, which is more favorable to Notch signaling, and determines ERK signaling by either VEGFR-3 or VEGFR-2 in the presence of VEGF-C or VEGF-A. This addresses the notion that CLEC14A regulates the transcription of *VEGFR-3* and *VEGFR-2* by controlling Notch-mediated signals.

CLEC14A deficiency results in abnormal tumor vasculature, hemorrhage, and reduced survival of tumor-bearing mice. EC-specific deletion of *VEGFR-3* increases tumor microvessel density (5, 21), strongly implicating the role of VEGFR-3 (and by extension VEGFR-2) in tumor angiogenesis. To test whether CLEC14A regulates tumor angiogenesis through modulation of VEGFR-3 and VEGFR-2, we injected B16F10 melanoma or Lewis lung carcinoma (LLC) cells into the abdomens of 6-week-old WT and CLEC14A-KO mice and evaluated tumor growth, tumor microvessel density, and survival rates. Tumor growth rates were approximately 50% lower in CLEC14A-KO mice than in WT mice for both tumor cell lines (Figure 5, A and B). Despite reduced tumor growth rates, survival was lower in CLEC14A-KO mice. Specifically, CLEC14A-KO mice died before tumors reached 4,000 mm³ in size, at which point the mice were sacrificed for ethical reasons (Figure 5, C and D).

To understand this discrepancy between reduced tumor growth and survival of CLEC14A-KO mice, we analyzed the peritumoral microvasculature of the tumors, including vessel density and stability. High tumor vessel density was detected by immunostaining with CD31 in both B16F10- and LLC-derived tumors (Figure 5, E–J). However, NG2 expression relative to CD31 expression was lower in the B16F10 and LLC tumor vessels of CLEC14A-KO mice (Figure 5, G and J), suggesting reduced pericyte coverage and greater vascular leakage. Immunostaining of both tumor types for CD31 and lectin, combined with prior i.v. FITC-dextran injection, revealed that tumor microvessels in the absence of CLEC14A were highly permeable, as evidenced by greater spreading of FITC-dextran around vessels (Figure 5, K–P). Furthermore, we evaluated vasculature integrity by analyzing α–smooth muscle actin (α-SMA, a perivascular cell marker) and collagen type IV (a component of the basement membrane) coverage in both tumor types, because previous reports have shown that loss of these proteins determines whether tumor angiogenesis promotes or suppresses tumor growth. Confocal images demonstrated reduced α-SMA coverage in CD31-positive vessels in CLEC14A-KO mice compared with that seen in WT mice (Supplemental Figure 14, A–F). Furthermore, collagen type IV degradation was more pronounced in B16F10 and LLC tumors from CLEC14A-KO mice than in those from WT mice (Supplemental Figure 14, G–L). To assess the effects of these changes in the microvascular structure on the tumor microenvironment, we evaluated tumor hypoxia by immunostaining with hypoxyprobe and found that tumors in CLEC14A-KO mice were highly deprived of oxygen (Supplemental Figure 15, A–F). We also observed severe hemorrhaging during removal of both tumor types from CLEC14A-KO mice but not from WT mice. Moreover, i.v. injection of Evans blue dye revealed increased extravasation from the tumor masses obtained from KO mice (Supplemental Figure 16, A and B). Immunostaining revealed higher VEGFR-2 expression in the vessels of both tumor types from CLEC14A-KO mice, consistent with our data from embryos and retinae (Supplemental Figure 17, A–F).
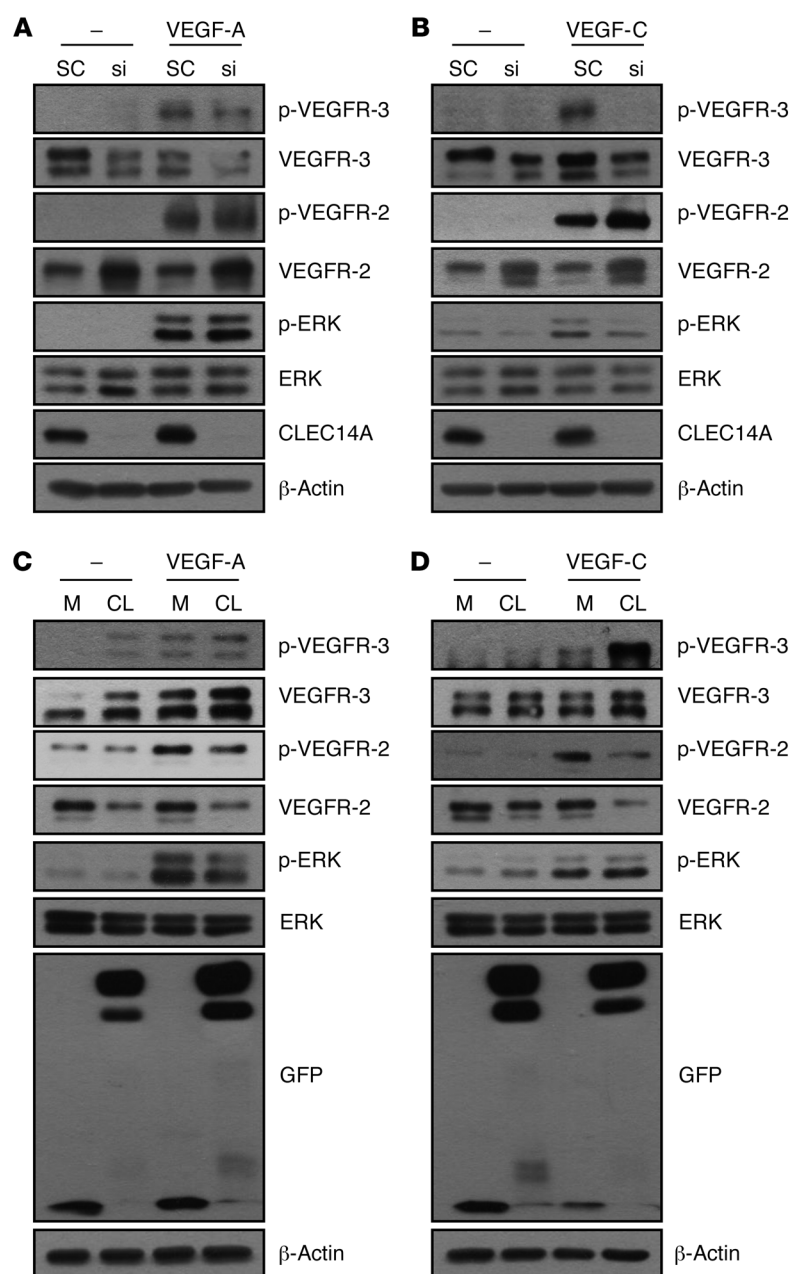
Figure 4. Silencing or overexpression of CLEC14A regulates the phosphoactivation of VEGFR-3 and VEGFR-2 and their downstream signaling upon stimulation with VEGF-C or VEGF-A in HDBECs. (**A**) Decreased phosphoactivation and expression of VEGFR-3 and increased phosphoactivation and expression of VEGFR-2 following increased phosphoactivation of ERK in HDBECs after knockdown of CLEC14A using siRNA (si) (50 nM) and treatment with 50 ng/ml VEGF-A for 5 minutes. (**B**) Decreased phosphoactivation and expression of VEGFR-3 following decreased phosphoactivation of ERK and increased phosphoactivation and expression of VEGFR-2 in HDBECs after knockdown of CLEC14A using siRNA (50 nM) and treatment with 100 ng/ml VEGF-C for 15 minutes. (**C**) Elevated phosphoactivation and expression of VEGFR-3 and reduced phosphoactivation and expression of VEGFR-2 following decreased phosphoactivation of ERK in HDBECs after overexpression of GFP-tagged CLEC14A, together with VEGF-A (50 ng/ml) for 5 minutes in HDBECs (GFP-Mock and GFP-CLEC14A-FL). (**D**) Enhanced phosphoactivation and expression of VEGFR-3 following increased phosphoactivation of ERK and decreased phosphoactivation and expression of VEGFR-2 after overexpression of GFP-tagged CLEC14A, together with VEGF-C (100 ng/ml) treatment for 15 minutes in HDBECs (GFP-Mock and GFP-CLEC14A-FL). All experiments were repeated in at least 4 different sets. M, mock transfected; CL, transfected with CLEC14A.

We hypothesized that these abnormal tumor microvessel characteristics in CLEC14A-KO mice enhance the metastatic potential. Footpad injection of B16BL6 melanoma cells resulted in greater lung metastases in CLEC14A-KO mice than was observed in WT mice (Figure 5, Q and R). Furthermore, lung colonization of i.v. injected B16BL6 melanoma cells was greater in CLEC14A-KO mice (Figure 5, S and T). Collectively, these results indicate that *Clec14a* deletion promotes excessive and unstable tumor angiogenesis, resulting in a higher metastatic potential as well as reduced survival.

Inhibition of VEGFRs, particularly VEGFR-2, efficiently suppresses tumor growth and enhances survival of CLEC14A-KO mice. Considering the effects of *Clec14a* deletion on VEGFR-2 expression, we examined whether administration of the VEGFR tyrosine kinase inhibitor and the clinical antitumor agent sunitinib or the VEGFR-2–specific

inhibitor DMH4 rescued the deleterious effects of CLEC14A KO. Administration of sunitinib or DMH4 further reduced tumor growth in CLEC14A-KO mice (Figure 6, A and B) and reversed the reduced viability of CLEC14A-KO mice (Figure 6C), suggesting that VEGFR-2 overexpression, along with the loss of CLEC14A, is responsible for the earlier death of tumor-bearing CLEC14A-KO mice. Furthermore, the severe hemorrhaging observed during the removal of tumors in vehicle-treated (DMSO-treated) CLEC14A-KO mice was reduced in CLEC14A-KO mice treated with sunitinib or DMH4 (Figure 6D). Reduced vessel density and FITC permeability were also observed in tumors of CLEC14A-KO mice following sunitinib or DMH4 treatment (Figure 6, E–G). Collectively, these data indicate that abnormal and unstable vessel characteristics as well as reduced survival upon deletion of *Clec14a* could be efficiently rescued by inhibition of VEGFR-2 signaling.

Discussion

We identified CLEC14A as a regulator of developmental angiogenesis and lymphangiogenesis as well as pathological angiogenesis. CLEC14A acts indirectly by modulating VEGFR-2 signaling through molecular interaction with VEGFR-3. Global CLEC14A KO in mice led to increased developmental angiogenesis and lymphangiogenesis as well as pathogenic angiogenesis. Moreover, these effects were associated with the loss of CLEC14A–VEGFR-3 interaction following impaired expression and phosphoactivation of VEGFR-3 as well as phosphoactivation and elevation of VEGFR-2 expression. In addition to excessive angiogenesis, loss of CLEC14A disrupted vascular integrity, possibly through the loss of pericytes, vascular smooth muscle cells, and collagen type IV. Furthermore, CLEC14A deficiency led to the formation of abnormal jugular lymph sacs and increased lymphangiogenesis. Lack of CLEC14A resulted in reduced viability of tumor-bearing mice, despite lower tumor growth rates. This reduced viability may have resulted from compromised vascular integrity and concomitant hemorrhage. Further substantiating the influence of VEGFR signaling in these deleterious effects of CLEC14A deficiency, a VEGFR kinase inhibitor and a specific VEGFR-2 inhibitor rescued vessel integrity and the reduced viability of tumor-bearing CLEC14A-KO mice. These findings strongly suggest that CLEC14A regulates blood and lymphatic vascular homeostasis and integrity during developmental and pathogenic angiogenesis as well as lymphangiogenesis.

Global deletion of *Clec14a* resulted in a hypervascular postnatal retina, similar to that observed in endothelium-specific *VEGFR-3*–KO and VEGF/VEGFR-2–overexpressing mice (3, 5, 22–24). Moreover, deletion of *Clec14a* resulted in jugular lymph sac and lymphatic vessel enlargement and increased lymphatic vessel density, analogous to what was observed in mice with a VEGFR-3 ligand–binding domain with an inactivation point mutation (25) and in mice with overexpression of VEGF or VEGFR-2 (26, 27) and opposite to what was observed in mice with a LYVE-1–specific *VEGFR-2* deletion, suggesting a close relationships among CLEC14A, VEGFR-3, and VEGFR-2 (28, 29). Pharmacological inhibition and genetic deletion experiments have demonstrated strong crosstalk between VEGF-A/VEGFR-2 and VEGF-A/VEGFR-3 signaling (4). Genetic deletion of *VEGFR-3* upregulates VEGFR-2 expression in vivo, whereas VEGFR-2 upregulation suppresses VEGFR-3 expression, suggesting that VEGFR-3 is a negative regulator of VEGFR-2 signaling (3, 5). Considering the phenotypic and functional similarities of our demonstration and findings of previous studies showing molecular and genetic controls of VEGFR-3 and VEGFR-2, we propose that CLEC14A acts as a positive regulator of VEGFR-3, which in turn guides appropriate and functional angiogenesis and lymphangiogenesis mediated by VEGFR-3 and VEGFR-2. In the absence of CLEC14A and with concomitant loss of the CLEC14A–VEGFR-3 complex, reduced VEGFR-3 activity and VEGFR-2 overexpression result in uncontrolled and functionally incomplete angiogenesis and abnormal lymphangiogenesis.

VEGFR-3 and VEGFR-2 signaling in BECs and LECs is regulated by various factors, including VEGF ligands (VEGF-A, VEGF-C, VEGF-D, and VEGF-E) (30–32). ERK signaling is activated by both VEGF-C/VEGFR-3 and VEGF/VEGFR-2 signaling (33). Distinct phosphorylation of ERK by CLEC14A modulation upon stimulation with VEGF-A or VEGF-C indicates that CLEC14A regulates VEGF-C/VEGFR-3 and VEGF/VEGFR-2 signaling, though further investigation of covalent crosslinking of VEGFR-2 and VEGFR-3 in the presence of VEGF or VEGF-C will answer the question of whether CLEC14A determines VEGFR-2/-3 heterodimerization by VEGF-A or VEGF-C. A consistent decrease in Notch signaling by CLEC14A silencing indicates that VEGF-C/VEGFR-3 signaling dominates Notch signaling compared with VEGF/VEGFR-2 signaling. Consistent with a previous study showing that Notch directly binds and regulates VEGFR-3 expression following alteration of VEGF responsiveness, we found that CLEC14A deficiency reduced VEGFR-3 expression following Notch expression, which in turn reduced VEGF-C responsiveness to VEGFR-3, as shown by reduced VEGFR-3 internalization by VEGF-C. The inverse pattern of endocytosed VEGFR-3 and VEGFR-2 in CLEC14A-deficient BECs and LECs upon VEGF-A and VEGF-C stimulation suggests that CLEC14A deletion does not determine the cell-surface expression of VEGFR-3. Our data suggest that CLEC14A induces a putative loss of VEGFR-3, thereby modulating VEGF/VEGFR-2 signaling as well as Notch and Notch target gene expression, which results in increased blood and lymphatic vessel density, hyperplasia, and enlargement of vessels. These effects may depend on the deficient expression of Notch and multiple Notch target genes that regulate VEGFR-3 transcription (34, 35), as *Clec14a* deletion decreased the expression of these critical downstream effectors of blood and lymphatic vascular growth.

VEGFR-2 signaling in BECs and LECs is regulated by a variety of membrane-spanning proteins such as claudin-like protein 24, ephrin B2, and neuropilin 1, which interact with VEGFR-2 or act as coreceptors to enhance VEGFR-2 affinity for VEGF-A (36). VEGF-A/VEGFR-2 signaling is also believed to be regulated by CLEC14A and MMRN2, although little information on CLEC14A effects was available prior to our study. Previous studies showed that MMRN2 binds with VEGF-A/-C, acting as a negative regulator of VEGF-A/VEGFR-2 signaling (37, 38). In line with findings that MMRN2 is downregulated by VEGF-A treatment and our demonstration that MMRN2 expression was reduced and phosphoactivation of VEGFR-2 was increased by *Clec14a* silencing in the absence or presence of VEGF-A, we consider that VEGF-A/VEGFR-2 signaling may be enhanced, as CLEC14A reduces MMRN2 expression, which then increases the availability of VEGF-A/VEGF-C to interact with VEGFR-2, concomitantly with the loss of VEGFR-3, which allows VEGFR-2 to interact with VEGF-A/VEGF-C and its molecular partners, thereby enhancing VEGFR-2 signaling (3, 5). Moreover, VEGFR-2 expression is autoregulated through an interaction with VEGF, translocating itself to the nucleus and binding to the proximal promoter region (39). Therefore, enhanced VEGFR-2 expression and activity appears to have resulted from the coincident failure of CLEC14A–VEGFR-3 complex formation, loss of VEGFR-3, loss of MMRN2, concomitant disinhibition of interactions between VEGFR-2 and membrane-bound coregulators, and autoregulation of VEGFR-2 by VEGF ligand.

According to recent reports, higher CLEC14A expression is directly associated with longer survival of patients with aggressive carcinomas such as clear-cell renal cell carcinoma and non–small-cell lung carcinoma (40, 41). This favorable clinical
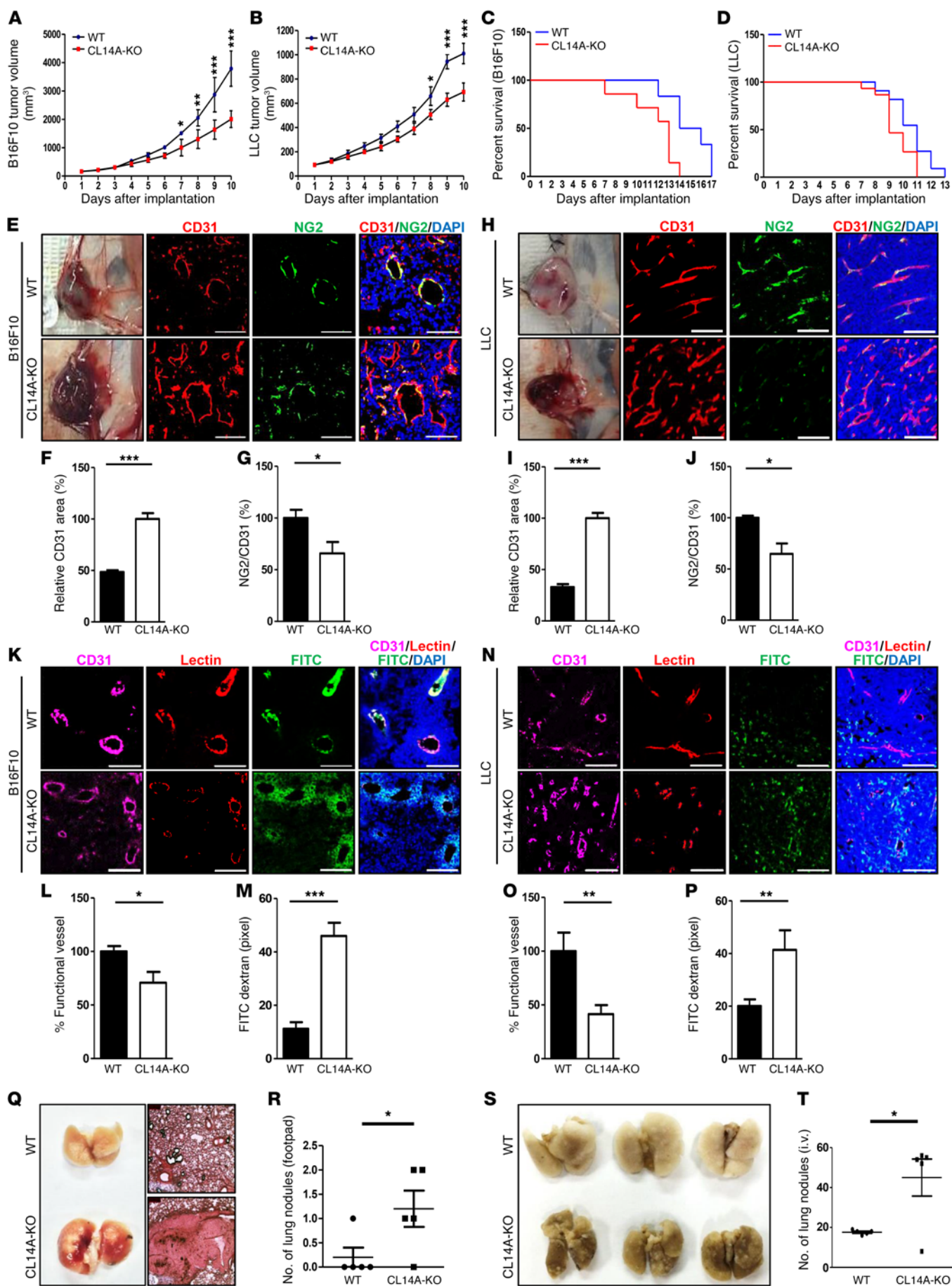
Figure 5. *Clec14a* deletion inhibits tumor growth but reduces mouse survival by enhancing the density of hemorrhage-prone tumor vessels.
(**A** and **B**) Growth curves of B16F10 and LLC tumors following s.c. injection of tumor cells into WT and CLEC14A-KO mouse abdomens. *n* = 6 per group. (**C** and **D**) Survival curves of WT and CLEC14A-KO mice implanted with B16F10 or LLC tumors. *n* = 3 per group. (**E**–**G**) Images of B16F10 tumors showing severe hemorrhage in CLEC14A-KO mice but only mild hemorrhage in WT mice. Immunostaining of B16F10 tumor sections (blood vessels, CD31; pericytes, NG2; nuclei, DAPI) and quantification of the relative CD31-positive area and NG2/CD31 ratio. (**H**–**J**) Images of LLC tumors showing severe hemorrhaging in CLEC14A-KO mice but mild hemorrhaging in WT mice. Immunostaining of LLC tumor sections and quantification of the relative CD31-positive area and NG2/CD31 ratio. (**K**–**M**) Images of B16F10 tumor vessels (CD31-positive, magenta) showing poor vascular perfusion (Lectin, red) and FITC-dextran leakage (FITC, green) in CLEC14A-KO mice compared with WT mice, and quantification of functional vessels (percentage of all CD31-positive vessels) and FITC-dextran leakage (pixels) in CLEC14A-KO mice relative to WT mice. *n* = 6 per group. Scale bars: 100 μm. (**N**–**P**) Images of LLC tumor vessels (CD31-positive), poor vascular perfusion (Lectin), and FITC-dextran leakage (FITC) in CLEC14A-KO mice relative to WT mice, and quantification of functional vessels (percentage of all CD31-positive vessels) and FITC-dextran leakage (pixels) in CLEC14A-KO mice relative to WT mice. *n* = 6 per group. Scale bars: 100 μm. (**Q**) Images of H&E-stained lungs from WT and CLEC14A-KO mice injected with B16BL6 into the footpads. *n* = 6 per group. Magnification: ×10. (**R**) Quantification of metastatic lung nodules in WT and CLEC14A-KO mice. *n* = 6 per group. (**S** and **T**) Image and quantification of metastatic lung nodules in WT and CLEC14A-KO mice i.v. injected with B16BL6. *n* = 6 per group.*$P < 0.05$, **$P < 0.005$, and ***$P < 0.0001$, by paired, 2-tailed Student's *t* test. Error bars represent the mean ± SD.

outcome is consistent with our finding that CLEC14A-KO mice implanted with tumors died earlier than did WT mice. Hemorrhagic shock leading to a systemic inflammatory response and multiple organ failure is a leading cause of cancer-related deaths (42, 43). Our previous study showed localization of CLEC14A in the vascular intercellular boundary between ECs and demonstrated that CLEC14A interacts with other proteins through the C-type lectin-like domain (14). Thus, a concentration of CLEC14A at EC junctions may be important for the formation of a well-organized vascular network. Conversely, impaired vascular integrity and the resultant hemorrhaging may have stemmed from weakened junctions upon the loss of C-type lectins as well as enhanced VEGFR-2 activity, which results in unstable and increased tumor angiogenesis (44, 45), upon the loss of CLEC14A–VEGFR-3 interaction.

Tumor angiogenesis is a major therapeutic target for cancer treatment, because tumors require vigorous angiogenesis to grow beyond a certain size (6, 7). Many studies and clinical trials have evaluated tumor responses to agents targeting VEGF/VEGFR-2 signaling (46–50). Recovery of functional vessels and survival of CLEC14A-KO mice by VEGFR-2 inhibitor treatment substantiate the role of CLEC14A in the regulation of VEGFR-2 and underscore the potential clinical relevance of CLEC14A expression in tumor angiogenesis. In a recent study, reduced tumor growth and endothelial coverage with reduced vessel density were observed in LLC tumor masses implanted into CLEC14A-KO mice (51), which is consistent with our results in both B16F10 and LLC tumor masses, except for the vessel density. Regarding the increased angiogenesis during development and the enhanced VEGFR-2 expression upon

deletion of *Clec14a*, increased vessel density following severe hemorrhaging appears more reliable. While the greater hemorrhagic potential of tumors in CLEC14A-KO mice is a possible cause of early death, we cannot exclude other potential causes, such as the inflammatory response to hemorrhagic shock or B16BL6 cell infiltration of the lungs (Figure 5Q), particularly since both VEGFR-3 and the CLEC14A paralog thrombomodulin regulate sepsis (52–54). Further immunological analysis of CLEC14A-deficient mice is required to determine the precise cause of early death.

Interestingly, our data and previous reports by Noy et al. (55) have two opposite outcomes. First, Noy et al. reported decreased sprouting in contrast to the increased sprouting observed in our aortic ring assay. Second, both studies generated the same results of reduced tumor growth rates, while demonstrating opposite tumor microvasculature phenotypes; specifically, Noy et al. observed reduced tumor vessel density in LLC tumor masses, whereas we noted increased tumor vessel density with leakiness and poor coverage in both B16F10 and LLC tumor masses. We obtained consistent results of increased aortic sprouting and increased blood vasculature in peritumoral regions. Further detailed study is required to elucidate the reasons for these differing results.

Overall, our findings suggest that CLEC14A regulates developmental angiogenesis and lymphangiogenesis as well as pathological angiogenesis by modulating the VEGF-C/VEGFR-3 and VEGF/VEGFR-2 pathways through a molecular interaction with VEGFR-3. These results implicate CLEC14A as an important contributor to the pathogenesis of diseases associated with neovascularization, such as OIR and cancer, through regulation of the VEGF/VEGFR-2/VEGFR-3 pathways. Regulation of CLEC14A may be a promising approach for the treatment of angiogenesis-related disorders.

Methods

Cell culture. ECs were isolated from HUVECs using collagenase as described previously (56) and cultured on gelatin-coated plates in Medium 199 (Invitrogen, Thermo Fisher Scientific) supplemented with 20% FBS, 3 ng/ml basic FGF (bFGF) (R&D Systems), 100 U/ml penicillin-streptomycin, and 5 U/ml heparin. Cells were collected by trypsinization and used for assays up to passage 7. HDBECs and HDLECs were purchased from PromoCell (catalogs C-12211 and C-12216, respectively) and cultured in EGM-2 (Lonza; catalog cc-4176). B16F10 and LLCs were purchased from ATCC and cultured in DMEM with 10% FBS. The B16BL6 cell line was purchased from the Korean Cell Line Bank (KCLB No. 80006) and cultured in DMEM with 10% FBS.

Generation of CLEC14A-KO mice. All mice were maintained on a C57BL/6 background and used between 6 and 8 weeks of age. The CLEC14A clone was obtained from the RPCI-22 Mouse 129S6/SvEvTAC Taconic BAC Library (https://bacpacresources.org), and the Southern blot probe was synthesized to test the probe in ES cell screening. A pgkTK vector was used to generate a CLEC14A-KO mouse construct. CLEC14A-KO mice were generated through homologous recombination of *Clec14a* and LacZ+Neo in a BacVac cassette.

Antibodies. The following primary antibodies were used: CD31 (BD Pharmingen; catalog 550274); NG-2 (EMD Millipore; catalog ab5320); CLEC14A (R&D Systems, catalog AF4968; Santa Cruz Biotechnology
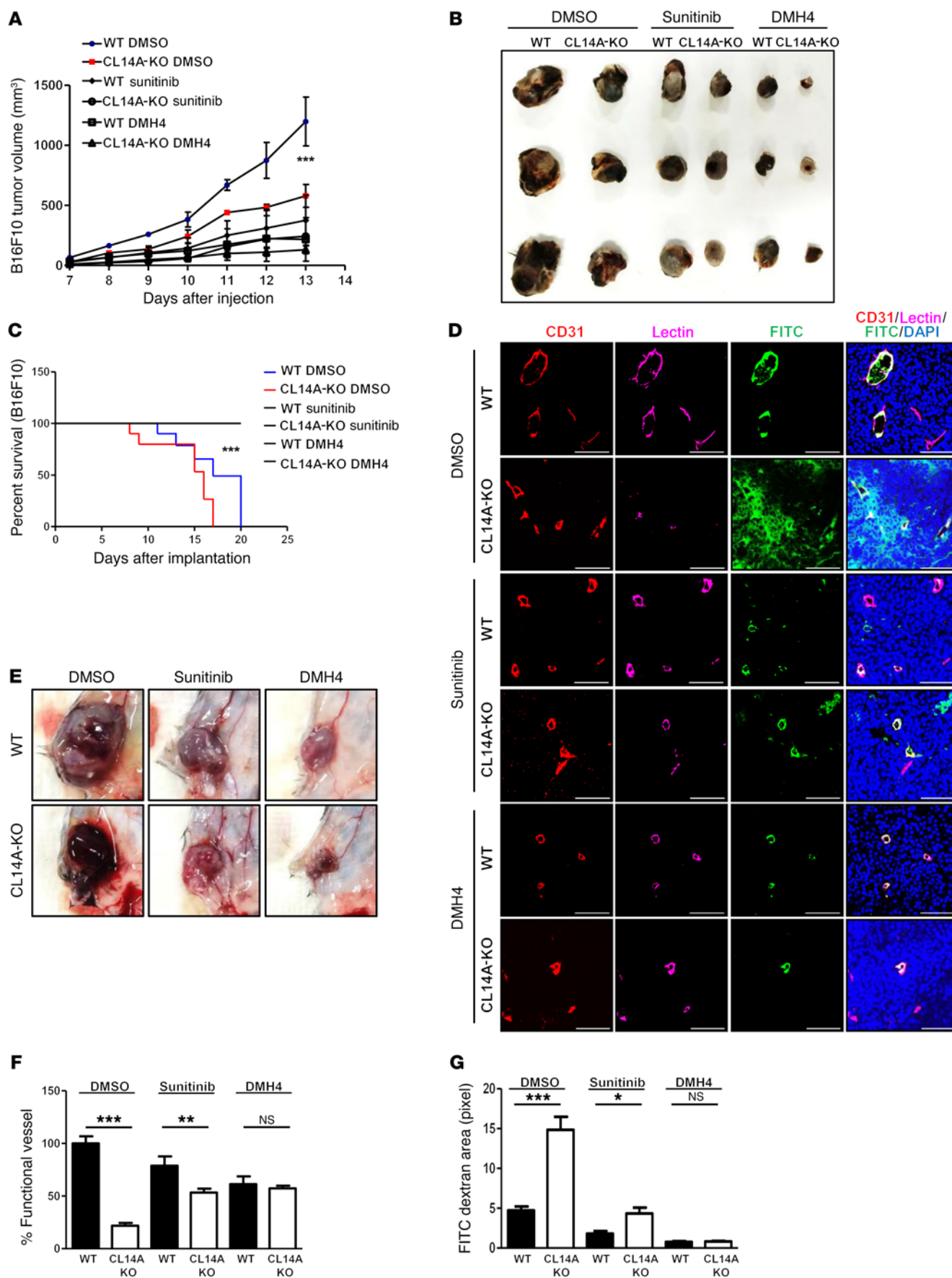
Figure 6. VEGFR-2 inhibitors suppress tumor growth, increase the number of functional vessels, and improve the survival of tumor-bearing CLEC14A-KO mice. (A) Growth curves of B16F10-derived tumors treated with vehicle (DMSO), sunitinib, or DMH4. n = 6 per group. (**B**) Size of captured B16F10 tumors under the different treatment conditions. (**C**) Survival curves of B16F10-injected WT and CLEC14A-KO mice treated with vehicle, sunitinib, or DMH4. n = 6 per group. (**D**) Images of B16F10 tumor masses before capture from WT and CLEC14A-KO mice treated with DMSO, sunitinib, or DMH4. (**E**) Immunostaining for CD31 and lectin as well as FITC-dextran and DAPI staining showing reduced leakage and increased numbers of functional vessels in mice treated with sunitinib or DMH4 compared with those treated with vehicle. Scale bars: 100 μm. (**F** and **G**) Quantification of functional vessels and FITC-dextran leakage in tumors from WT and CLEC14A-KO mice treated with DMSO, sunitinib, or DMH4. n = 6 per group. *P < 0.05, **P < 0.005, and ***P < 0.0001, by paired, 2-tailed Student's t test. Error bars represent the mean ± SD.

Inc., catalogs sc-246295 and sc-246296; Abcam, catalog Ab73087); MMRN2 (Santa Cruz Biotechnology Inc.; catalog sc-54120); LYVE-1 (AngioBio; catalog 11-034); VEGFR-2 (Cell Signaling Technology; catalog 2479); p–VEGFR-3 (Cell Applications Inc.; catalog CY1115); VEGFR-3 (R&D Systems, catalogs AF349 for human and AF743 for mouse; Santa Cruz Biotechnology Inc., catalog sc321); collagen type IV (Cosmo Bio; catalog LSL-LB-1407); PH3 (EMD Millipore; catalog 66-570); FITC (catalog FD40S), α-SMA (catalog F3777), X-gal (catalog 7240-90-6), and DAPI (catalog D9542) (Sigma-Aldrich); EEA1 (Santa Cruz Biotechnology Inc.; catalog sc-33585); β-actin (Thermo Fisher Scientific; catalog MA5-15739); and phosphorylated eNOS (p-eNOS), eNOS, p–VEGFR-2, VEGFR-2, p-ERK, and ERK (Cell Signaling Technology; catalogs 9571, 9572, 2478, 2479, 9106, and 9102). The secondary antibodies used were Alex Fluor 350 (catalog A21093, A31552), 488 (catalog A11006), 594 (catalog A21209), 680 (catalog A100043, A21084) (Invitrogen, Thermo Fisher Scientific).

RNA interference and RT-PCR. HUVECs were transfected for 3 hours with scrambled siRNA or CLEC14A siRNA using lipofectamine (Invitrogen, Thermo Fisher Scientific) and assayed 36 hours after transfection. The sequence of the CLEC14A siRNA (5′-CAAU-CAGGGUCGACGAGAA-3′) was designed by Dharmacon Inc. The VEGFR-3 siRNA from the ON-TARGETplus SMARTpool was used for VEGFR-3 knockdown (Dharmacon Inc.; catalog L-003138-00). For RT-PCR assays, total RNA (isolated from HUVECs transfected with scrambled siRNAs or CLEC14A siRNA, from P4 MLECs, or from P6 WT and CLEC14A-KO mouse hyaloid vessels) was reverse transcribed to cDNA and amplified with the primers listed in Supplemental Table 2 on a PikoReal 96 Real-Time PCR System (Thermo Fisher Scientific) using Maxima SYBR Green/ROX qPCR Master Mix (Thermo Fisher Scientific; catalog K0221). All RT-PCR assays were performed in quintuplicate in at least 3 independent experiments using 2 different samples.

Aortic ring assay. The aortic ring assay was performed as described previously (57). In brief, aortic rings were isolated from P7 WT and CLEC14A-KO littermates and cut to a fixed size in PBS. Growth factor–reduced Matrigel (50 μl; BD Biosciences; catalog 354230) was spread onto each well of 24-well plates, and the plates were incubated at 37°C for 10 to 15 minutes to allow the matrix to polymerize. The aortic rings were then placed on the matrix (1 per well), and 50 μl Matrigel was applied to cover each ring. The plates were incubated at 37°C for 10 to 15 minutes to allow the newly poured Matrigel to polymerize. Each encased ring was cultured in

1 ml Opti-MEM culture medium (Gibco, Thermo Fisher Scientific) supplemented with 2.5% FBS and 50 ng/ml VEGF-A. The medium was changed on day 3 and then every other day.

Matrigel plug assay. Six-week-old WT and CLEC14A-KO mice were injected s.c. with 0.6 ml Matrigel containing 100 ng VEGF-A and 10 U heparin. The injected Matrigel rapidly formed a single, solid gel plug. After 5 or 10 days, the skin of the mouse was pulled back to expose the Matrigel plug, which remained intact. Hb within the plug was measured using the Drabkin Reagent Kit 525 (Sigma-Aldrich) and quantified by comparing with plugs with known Hb concentrations run in parallel. To identify infiltrating ECs, IHC was performed on slices of the Matrigel plug using an anti-CD31 antibody (BD Biosciences).

OIR model. The OIR assay was performed as described previously (58). Mice at P7 were exposed to a hyperoxic atmosphere (75% O_2) for 5 days, followed by a return to normoxia for an additional 5 days. The mice were anesthetized and sacrificed using avertin. The eyes were removed and fixed in 4% paraformaldehyde (PFA) (pH 7.4) for 20 minutes at room temperature. The retinae were dissected, postfixed in 1% PFA for 1 hour, washed with PBS, permeabilized with PBS containing 1% Triton X-100 for 1 hour, incubated in blocking solution for 1 hour (all at room temperature), and incubated overnight in Alexa 488–conjugated isolectin GS-IB4 solution (Molecular Probes, Thermo Fisher Scientific) at 4°C. After 5 washes in PBS containing 1% Triton X-100, the retinae were flat mounted on slides and analyzed using an Olympus IX81-ZDC inverted fluorescence microscope and a confocal microscope (LSM 700 META; Carl Zeiss).

Tumor implantation. B16F10 murine melanoma cells or murine LLC cells (5 × 10⁵ cells; syngeneic with C57BL/6 mice) suspended in 100 μl HBSS were s.c. injected into the abdominal area of 6- to 7-week-old male WT and CLEC14A-KO mice. Also, B16BL6 cells were s.c. or i.v. injected into the footpad and tail vein, respectively. After tumors were detected, growth was monitored every day by measuring the length and width of the tumors using callipers. The tumor volume (mm³) was calculated using the following ellipsoid volume formula: $0.523 \times l \times w^2$, where l is the length and w is the width. The tumor masses were resected at the size of 1,000 mm³, and peritumoral regions were used for vascular phenotype analysis. The percentage of surviving mice was determined by monitoring the tumor volume (up to 4,000 mm³) over a period of 20 days.

Drugs. Sunitinib (Cayman Chemical; catalog 13159) and DMH4 (Tocris Bioscience; catalog 4471) were directly injected into the B16F10 and LLC tumor masses implanted into 6-week-old WT and CLE14A-KO mice.

Cryosectioning and immunofluorescence staining. Tissues were fixed in 4% PFA and PBS (pH 7.4) overnight at 4°C, rinsed with PBS at room temperature, incubated in 15% sucrose overnight at 4°C, and transferred to 30% sucrose at 4°C until the tissue sank. Fixed tissues were infiltrated with Tissue-Tek OCT embedding medium for 0.5 hours at room temperature, transferred to an embedding mold filled with OCT, frozen on dry ice, and stored at –70°C. Frozen sections (10- to 40-μm-thick) were cut at –20°C, and slides were stored at –70°C until use for immunostaining. In brief, the sections were prefixed in acetone for 0.5 hours at –70°C and briefly air dried. OCT was removed with flowing water. The sections were incubated in blocking solution for 1 hour at 37°C, incubated overnight in primary antibody (1:1,000) at 4°C, washed 3 times with 0.1% Triton X-100 in PBS (10 min/wash), incubated in secondary antibody

(1:1,000) overnight at 4°C, counterstained with DAPI (1 μg/ml), and washed 5 more times with 0.1% Triton X-100 in PBS (10 min/wash). All antibodies were dissolved in antibody diluent (Dako, Agilent Technologies). The sections were analyzed by fluorescence microscopy using an Olympus IX81-ZDC inverted fluorescence microscope or a confocal microscope (LSM 510 META and LSM 700 META; Carl Zeiss).

FITC-lectin perfusion assay. Functional tumor vessels were labeled in vivo by i.v. injection of 100 μl Biotinylated Lycopersicon Esculentum (Tomato) lectin (1 mg/ml; Vector Laboratories). After a circulation time of 30 minutes, the mice were anesthetized with avertin, and whole-body perfusion fixation was performed with 1% PFA. Tumors were excised and prepared for cryosectioning and immunofluorescence staining as described above.

Vessel density analyses. Vessel densities in tumors and retinae were determined using Multi Gauge Fujifilm and AngioTool (59).

Vascular permeability assay. Evans blue dye (30 mg/kg in 100 μl PBS; Sigma-Aldrich) was injected into the tail vein of CLEC14A-KO and WT littermates bearing B16F10 and LLC tumors. After 30 minutes, the mice were anesthetized by i.p. injection of avertin (125 mg/kg) and then perfused with 1% PFA for 1 to 2 minutes. The tumor were excised and dried at 60°C for 16 hours before weighing. Evans blue dye was extracted from the tumor samples in 1 ml formamide at 55°C for 16 hours and quantified by measuring the OD at 610 nm.

Statistics. Data are presented as the mean ± SD or SEM. Multiple group means were compared by 1-way ANOVA, followed by a 2-tailed Student's t test for pair-wise comparisons. Survival curves were plotted against time by the Kaplan-Meier method and compared by log-rank test analysis using StatView software (Abacus Concepts Inc.). A P value of less than 0.05 was considered significant.

Study approval. All mice were maintained in a laminar airflow cabinet under specific pathogen–free conditions. All facilities were approved by the Association of Assessment and Accreditation of Laboratory Animal Care, and all animal experiments were conducted under the institutional guidelines established for the Animal Care Facility at Yonsei University College of Medicine and the Yonsei Laboratory Animal Research Center (YLARC) at Yonsei University. Animal experiments were approved by the Yonsei Laboratory Animal Research Center (YLARC) at Yonsei University (Seoul, South Korea).

Author contributions

SWL and HJP designed the project and planned the experiments. SSR generated the CLEC14A-KO mice. SWL and HJP performed all experiments and quantifications. SWL and HJP analyzed and discussed the results. SWL, HJP, and YGK wrote the manuscript. NM revised manuscript and GYK made comments on experiments. JAP, JK, IKL, YMK made comments.

Acknowledgments

Address correspondence to: Young-Guen Kwon, Department of Biochemistry, College of Life Science and Biotechnology, Yonsei University, Seoul, 120-749, Republic of Korea. Phone: 82.2.2123.5697; E-mail: ygkwon@yonsei.ac.kr.

1. Kremer C, Breier G, Risau W, Plate KH. Up-regulation of flk-1/vascular endothelial growth factor receptor 2 by its ligand in a cerebral slice culture system. *Cancer Res.* 1997;57(17):3852–3859.

2. Dumont DJ, et al. Cardiovascular failure in mouse embryos deficient in VEGF receptor-3. *Science.* 1998;282(5390):946–949.

3. Zarkada G, Heinolainen K, Makinen T, Kubota Y, Alitalo K. VEGFR3 does not sustain retinal angiogenesis without VEGFR2. *Proc Natl Acad Sci USA.* 2015;112(3):761–766.

4. Benedito R, et al. Notch-dependent VEGFR3 upregulation allows angiogenesis without VEGF-VEGFR2 signalling. *Nature.* 2012;484(7392):110–114.

5. Tammela T, et al. VEGFR-3 controls tip to stalk conversion at vessel fusion sites by reinforcing Notch signalling. *Nat Cell Biol.* 2011;13(10):1202–1213.

6. Folkman J. Role of angiogenesis in tumor growth and metastasis. *Semin Oncol.* 2002;29(6 Suppl 16):15–18.

7. Saharinen P, Eklund L, Pulkki K, Bono P, Alitalo K. VEGF and angiopoietin signaling in tumor angiogenesis and metastasis. *Trends Mol Med.* 2011;17(7):347–362.

8. Mura M, et al. Identification and angiogenic role of the novel tumor endothelial marker CLEC14A. *Oncogene.* 2012;31(3):293–305.

9. Zelensky AN, Gready JE. The C-type lectin-like domain superfamily. *FEBS J.* 2005;272(24):6179–6217.

10. Isermann B, et al. Endothelium-specific loss of murine thrombomodulin disrupts the protein C anticoagulant pathway and causes juvenile-onset thrombosis. *J Clin Invest.* 2001;108(4):537–546.

11. Shi CS, et al. Lectin-like domain of thrombomodulin binds to its specific ligand Lewis Y antigen and neutralizes lipopolysaccharide-induced inflammatory response. *Blood.* 2008;112(9):3661–3670.

12. Nanda A, et al. Tumor endothelial marker 1 (Tem1) functions in the growth and progression of abdominal tumors. *Proc Natl Acad Sci USA.* 2006;103(9):3351–3356.

13. Geijtenbeek TB, Gringhuis SI. Signalling through C-type lectin receptors: shaping immune responses. *Nat Rev Immunol.* 2009;9(7):465–479.

14. Rho SS, et al. Clec14a is specifically expressed in endothelial cells and mediates cell to cell adhesion. *Biochem Biophys Res Commun.* 2011;404(1):103–108.

15. Colladel R, et al. MULTIMERIN2 binds VEGF-A primarily via the carbohydrate chains exerting an angiostatic function and impairing tumor growth. *Oncotarget.* 2016;7(2):2022–2037.

16. Zanivan S, et al. SILAC-based proteomics of human primary endothelial cell morphogenesis unveils tumor angiogenic markers. *Mol Cell Proteomics.* 2013;12(12):3599–3611.

17. Masiero M, et al. A core human primary tumor angiogenesis signature identifies the endothelial orphan receptor ELTD1 as a key regulator of angiogenesis. *Cancer Cell.* 2013;24(2):229–241.

18. Delcourt N, et al. Targeted identification of sialoglycoproteins in hypoxic endothelial cells and validation in zebrafish reveal roles for proteins in angiogenesis. *J Biol Chem.* 2015;290(6):3405–3417.

19. Noy PJ, Swain RK, Khan K, Lodhia P, Bicknell R. Sprouting angiogenesis is regulated by shedding of the C-type lectin family 14, member A (CLEC14A) ectodomain, catalyzed by rhomboid-like 2 protein (RHBDL2). *FASEB J.* 2016;30(6):2311–2323.

20. Caldwell RB, et al. Vascular endothelial growth factor and diabetic retinopathy: pathophysiological mechanisms and treatment perspectives. *Diabetes Metab Res Rev*. 2003;19(6):442–455.

21. Hanahan D, Folkman J. Patterns and emerging mechanisms of the angiogenic switch during tumorigenesis. *Cell*. 1996;86(3):353–364.

22. Coultas L, Chawengsaksophak K, Rossant J. Endothelial cells and VEGF in vascular development. *Nature*. 2005;438(7070):937–945.

23. Flamme I, von Reutern M, Drexler HC, Syed-Ali S, Risau W. Overexpression of vascular endothelial growth factor in the avian embryo induces hypervascularization and increased vascular permeability without alterations of embryonic pattern formation. *Dev Biol*. 1995;171(2):399–414.

24. Larcher F, Murillas R, Bolontrade M, Conti CJ, Jorcano JL. VEGF/VPF overexpression in skin of transgenic mice induces angiogenesis, vascular hyperpermeability and accelerated tumor development. *Oncogene*. 1998;17(3):303–311.

25. Zhang L, et al. VEGFR-3 ligand-binding and kinase activity are required for lymphangiogenesis but not for angiogenesis. *Cell Res*. 2010;20(12):1319–1331.

26. Wirzenius M, et al. Distinct vascular endothelial growth factor signals for lymphatic vessel enlargement and sprouting. *J Exp Med*. 2007;204(6):1431–1440.

27. Nakao S, et al. Blood vessel endothelial VEGFR-2 delays lymphangiogenesis: an endogenous trapping mechanism links lymph- and angiogenesis. *Blood*. 2011;117(3):1081–1090.

28. Hong YK, et al. VEGF-A promotes tissue repair-associated lymphatic vessel formation via VEGFR-2 and the alpha1beta1 and alpha2beta1 integrins. *FASEB J*. 2004;18(10):1111–1113.

29. Dellinger MT, Meadows SM, Wynne K, Cleaver O, Brekken RA. Vascular endothelial growth factor receptor-2 promotes the development of the lymphatic vasculature. *PLoS One*. 2013;8(9):e74686.

30. Dixelius J, et al. Ligand-induced vascular endothelial growth factor receptor-3 (VEGFR-3) heterodimerization with VEGFR-2 in primary lymphatic endothelial cells regulates tyrosine phosphorylation sites. *J Biol Chem*. 2003;278(42):40973–40979.

31. Nilsson I, et al. VEGF receptor 2/-3 heterodimers detected in situ by proximity ligation on angiogenic sprouts. *EMBO J*. 2010;29(8):1377–1388.

32. Mäkinen T, et al. Isolated lymphatic endothelial cells transduce growth, survival and migratory signals via the VEGF-C/D receptor VEGFR-3. *EMBO J*. 2001;20(17):4762–4773.

33. Deng Y, Zhang X, Simons M. Molecular controls of lymphatic VEGFR3 signaling. *Arterioscler Thromb Vasc Biol*. 2015;35(2):421–429.

34. Shawber CJ, et al. Notch alters VEGF responsiveness in human and murine endothelial cells by direct regulation of VEGFR-3 expression. *J Clin Invest*. 2007;117(11):3369–3382.

35. Zheng W, et al. Notch restricts lymphatic vessel sprouting induced by vascular endothelial growth factor. *Blood*. 2011;118(4):1154–1162.

36. Koch S, Tugues S, Li X, Gualandi L, Claesson-Welsh L. Signal transduction by vascular endothelial growth factor receptors. *Biochem J*. 2011;437(2):169–183.

37. Lorenzon E, et al. MULTIMERIN2 impairs tumor angiogenesis and growth by interfering with VEGF-A/VEGFR2 pathway. *Oncogene*. 2012;31(26):3136–3147.

38. Zanivan S, et al. SILAC-based proteomics of human primary endothelial cell morphogenesis unveils tumor angiogenic markers. *Mol Cell Proteomics*. 2013;12(12):3599–3611.

39. Domingues I, Rino J, Demmers JA, de Lanerolle P, Santos SC. VEGFR2 translocates to the nucleus to regulate its own transcription. *PLoS One*. 2011;6(9):e25668.

40. Wozniak MB, et al. Integrative genome-wide gene expression profiling of clear cell renal cell carcinoma in Czech Republic and in the United States. *PLoS One*. 2013;8(3):e57886.

41. Pircher A, et al. Favorable prognosis of operable non-small cell lung cancer (NSCLC) patients harboring an increased expression of tumor endothelial markers (TEMs). *Lung Cancer*. 2013;81(2):252–258.

42. Kao RL, et al. Induction of acute lung inflammation in mice with hemorrhagic shock and resuscitation: role of HMGB1. *J Inflamm (Lond)*. 2014;11(1):30.

43. Yang R, et al. Anti-HMGB1 neutralizing antibody ameliorates gut barrier dysfunction and improves survival after hemorrhagic shock. *Mol Med*. 2006;12(4-6):105–114.

44. Chatterjee S, et al. Tumor VEGF:VEGFR2 autocrine feed-forward loop triggers angiogenesis in lung cancer. *J Clin Invest*. 2013;123(4):1732–1740.

45. Kerbel RS. Tumor angiogenesis. *N Engl J Med*. 2008;358(19):2039–2049.

46. Sitohy B, Nagy JA, Dvorak HF. Anti-VEGF/VEGFR therapy for cancer: reassessing the target. *Cancer Res*. 2012;72(8):1909–1914.

47. McMahon G. VEGF receptor signaling in tumor angiogenesis. *Oncologist*. 2000;5 Suppl 1:3–10.

48. Moreira IS, Fernandes PA, Ramos MJ. Vascular endothelial growth factor (VEGF) inhibition--a critical review. *Anticancer Agents Med Chem*. 2007;7(2):223–245.

49. Herold-Mende C, et al. Expression and functional significance of vascular endothelial growth factor receptors in human tumor cells. *Lab Invest*. 1999;79(12):1573–1582.

50. Ho VC, Duan LJ, Cronin C, Liang BT, Fong GH. Elevated vascular endothelial growth factor receptor-2 abundance contributes to increased angiogenesis in vascular endothelial growth factor receptor-1-deficient mice. *Circulation*. 2012;126(6):741–752.

51. Noy PJ, et al. Blocking CLEC14A-MMRN2 binding inhibits sprouting angiogenesis and tumour growth. *Oncogene*. 2015;34(47):5821–5831.

52. Zhang Y, et al. Activation of vascular endothelial growth factor receptor-3 in macrophages restrains TLR4-NF-κB signaling and protects against endotoxin shock. *Immunity*. 2014;40(4):501–514.

53. Iba T, Yagi Y, Kidokoro A, Fukunaga M, Fukunaga T. Increased plasma levels of soluble thrombomodulin in patients with sepsis and organ failure. *Surg Today*. 1995;25(7):585–590.

54. Ikezoe T. Thrombomodulin/activated protein C system in septic disseminated intravascular coagulation. *J Intensive Care*. 2015;3(1):1.

55. Noy PJ, et al. Blocking CLEC14A-MMRN2 binding inhibits sprouting angiogenesis and tumour growth. *Oncogene*. 2015;34(47):5821–5831.

56. Marin V, Kaplanski G, Grès S, Farnarier C, Bongrand P. Endothelial cell culture: protocol to obtain and cultivate human umbilical endothelial cells. *J Immunol Methods*. 2001;254(1-2):183–190.

57. Baker M, et al. Use of the mouse aortic ring assay to study angiogenesis. *Nat Protoc*. 2011;7(1):89–104.

58. Connor KM, et al. Quantification of oxygen-induced retinopathy in the mouse: a model of vessel loss, vessel regrowth and pathological angiogenesis. *Nat Protoc*. 2009;4(11):1565–1573.

59. Zudaire E, Gambardella L, Kurcz C, Vermeren S. A computational tool for quantitative analysis of vascular networks. *PLoS One*. 2011;6(11):e27385.